minerals

MDPI

Article

High Specific Activity of Radium Isotopes in Baryte from the Czech Part of the Upper Silesian Basin—An Example of Spontaneous Mine Water Treatment

Jakub Jirásek [1,*], Dalibor Matýsek [2], Petr Alexa [3], Michal Osovský [4], Radim Uhlář [5] and Martin Sivek [6]

[1] Department of Geological Engineering & ENET Centre, VŠB-Technical University of Ostrava, 17. listopadu 15/2172, 708 00 Ostrava-Poruba, Czech Republic
[2] Department of Geological Engineering & ICT Centre, VŠB-Technical University of Ostrava, 17. listopadu 15/2172, 708 00 Ostrava-Poruba, Czech Republic; dalibor.matysek@vsb.cz
[3] Department of Physics & ICT Centre, VŠB-Technical University of Ostrava, 17. listopadu 15/2172, 708 00 Ostrava-Poruba, Czech Republic; petr.alexa@vsb.cz
[4] OKD, a.s., ČSA Mine, ul. Čs. armády 1, 735 06 Karviná-Doly, Czech Republic; michal.osovsky@okd.cz
[5] Department of Physics, Faculty of Electrical Engineering and Computer Science, VŠB-Technical University of Ostrava, 17. listopadu 15/2172, 708 00 Ostrava-Poruba, Czech Republic; radim.uhlar@vsb.cz
[6] Department of Geological Engineering, Faculty of Mining and Geology, VŠB-Technical University of Ostrava, 17. listopadu 15/2172, 708 00 Ostrava-Poruba, Czech Republic; martin.sivek@vsb.cz
* Correspondence: jakub.jirasek@vsb.cz

Received: 17 December 2019; Accepted: 18 January 2020; Published: 25 January 2020

Abstract: Radium-bearing barytes (radiobarytes) have been known since the beginning of the 20th century. They are mainly found as precipitates of low-temperature hydrothermal solutions. In anthropogenic environments, they frequently occur as crusts on oil industry equipment used for borehole extraction, in leachates from uranium mill tailings, and as a by-product of phosphoric acid manufacturing. Recently, we recognized Ra-rich baryte as a precipitate in the water drainage system of a bituminous coal mine in the Czech part of the Upper Silesian Basin. The precipitate is a relatively pure baryte, with the empirical formula $(Ba_{0.934}Sr_{0.058}Ca_{0.051}Mg_{0.003})_{\Sigma 1.046}S_{0.985}O_{4.000}$. The mean specific activity of ^{226}Ra was investigated by the two-sample method and it equals 39.62(22) Bq/g, a level that exceeds known natural occurrences. The values for ^{228}Ra and ^{224}Ra are 23.39(26) Bq/g and 11.03(25) Bq/g. The radium content in the baryte is 1.071 ng/g. It is clear that the Ra-rich baryte results from the mixing of two different mine waters—brines rich in Ba, Sr, and isotopes ^{226}Ra and ^{228}Ra and waters that are affected by sulfide weathering in mine works. When this mixing occurs in surface watercourses, it could present a serious problem due to the half-life of ^{226}Ra, which is 1600 years. If such mixing spontaneously happens in a mine, then the environmental risks will be much lower and will be, to a great, extent eliminated after the closure of the mine.

Keywords: baryte; barium; radium; cation exchange; mine water

1. Introduction

The radium isotope ^{226}Ra is a daughter product of ^{230}Th alpha decay in the ^{238}U decay series, which is also known as the uranium or radium series. The radium isotopes ^{228}Ra and ^{224}Ra are the daughter products of ^{228}Ac, resp. ^{228}Th decay in the ^{232}Th decay series, also known as the thorium series [1]. Radium is enriched in some naturally occurring radioactive materials (NORMs), but even higher concentrations can be found in some technologically enhanced naturally occurring radioactive materials (TENORMs).

Among natural occurrences, the most common are trace amounts of radium in aquifers [2,3]. Increased concentrations have been reported in mineral and thermal waters [4–10] and in brines [11–14]. Among natural mineral phases, radium-rich baryte (also known as radian baryte or radiobaryte) is baryte that contains trace amounts of radium. The natural occurrences of radiobaryte were first noticed at the beginning of the 20th century. Such occurrences are connected with low-temperature hydrothermal fluorite-baryte mineralization [15,16], and the radioactivity can reach 8 Bq/g.

In the anthropogenic environment, the most common concentrator of radium, by far, is radium-rich baryte, followed by radium-rich gypsum [17]. These materials frequently occur as crusts on oil industry equipment used for borehole extraction [18–22], in leachates from uranium mill tailings [23–26], and as by-products of phosphoric acid manufacturing [27–30]. The radium content of these anthropogenic materials is much higher than that of natural phases and it can reach 1×10^3 Bq/g in the samples from the first source mentioned.

In both NORMs and TENORMs, the formation of Ra-rich baryte causes the removal of radium dissolved in water [31,32]. Experimental investigations of the formation of solid solutions between radium and baryte have proved that this process happens at fast kinetic rates [33,34] and, therefore, available radium can be fixed if enough Ba^{2+} and $SO_4{}^{2-}$ are available in solution.

The crusts of unknown minerals were found during a review of the water drainage system at the ČSA Mine, Doubrava Shaft (Figure 1), which extracts bituminous coal from the Karviná Formation of the Upper Silesian Basin, Czech Republic. The crusts were highly radioactive, emitting particles by alpha decay. Baryte was proven to be a major component of this incrustation, with radium content being responsible for the radioactivity. The aim of this paper is to characterize the genesis of this material, its composition, and the specific activity of the radium isotopes. The results will help to elucidate the behaviour and possible hazards of this potentially hazardous TENORM.

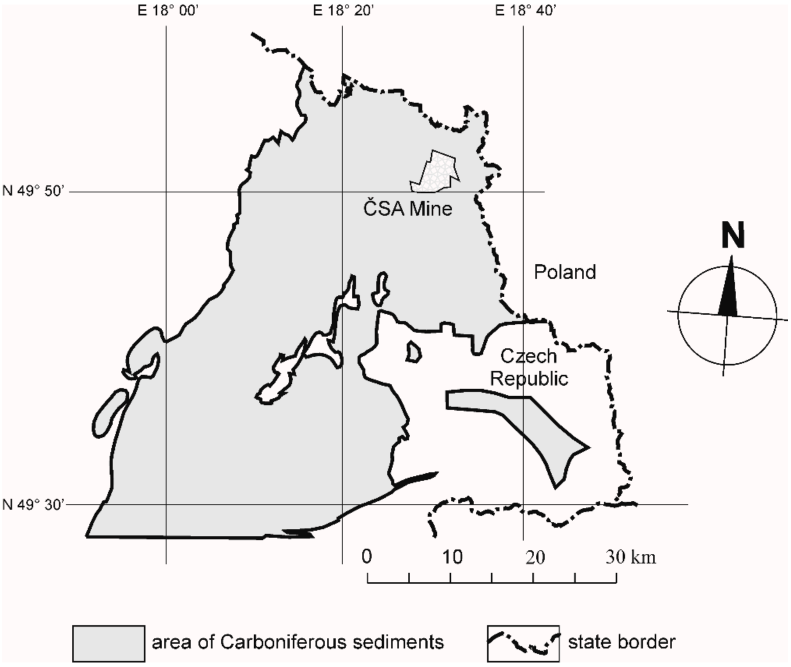

Figure 1. Schematic map of the Czech part of the Upper Silesian Basin showing the area of the ČSA Mine, where the investigated Ra-rich baryte comes from.

2. Geological Setting

2.1. The Upper Silesian Basin

The Upper Silesian Basin belongs to the eastern domain of the Central European Variscides. It is a typical foreland basin [35]. The post-erosional boundary of the basin has a roughly triangular shape that extends from Poland southward into the Czech Republic. The area of this important European bituminous coal basin exceeds 7400 km^2 [36].

The sedimentary sequence that fills the Czech part of the basin has been discussed by, e.g., [37,38]. Cyclic alternation of clastic sediments with coalbeds is typical for the whole sedimentary record [39]. Intercalations of volcanoclastic material are frequent [40]. The older type of sedimentation from the Serpukhovian stage contains marine horizons [39], while younger formations that range from the Bashkirian to early Kasimovian stage originate purely in terrestrial settings [41].

The basement of the basin is formed by the sedimentary cover of the Brunovistulicum and it is specifically formed by sediments of the Cambrian, Ordovician, Devonian, and Mississippian [42,43]. The basin fill is overlain primarily by Triassic, Neogene, and Quaternary deposits and Permian and Jurassic sedimentary sequences in the Polish part. The southern (Czech) part of the basin is overlain by Neogene deposits of the Carpathian Foredeep and it is overlain by nappes of the Outer Carpathians (Jurassic to Paleogene) further to the south [37].

2.2. Geochemical and Hydrogeochemical Background

While considering that uranium is a primary source of radium, it is necessary to mention that uranium minerals are not known in the Upper Silesian Basin. Local coal contains up to 44 ppm U and 24 ppm Th in coal ashes [44], which is not higher dramatically than the Clarke value for world bituminous coals—15 ppm for U and 23 ppm for Th [45]. Whether the uranium is bound to the organic or inorganic material in the coal is not yet known with certainty. The U and Th contents of sediments [46,47] and tuffs [47] have also been published. In such samples, both of the elements are present as the isomorphic admixtures, mostly in zircon and minerals of the monazite and apatite groups, U is probably also sorbed in clay minerals and/or organic matter.

The hydrogeological and hydrogeochemical conditions in the Czech part of the Upper Silesian Basin are known to be complex. The basin contains nine water-bearing systems at different stratigraphic levels [48] that differ in the contents of dissolved gases and elements.

The geochemistry and origin of the water have been studied, such as in a study by [49]. Four of the water-bearing systems that they noted are of interest for the purposes of this study. First, the systems are connate waters of the Miocene sea formation. Their total mineralization varies, with values up to 150 g/L. The systems are virtually sulfate and uranium free, and the Ba^{2+} content does not exceed 40 mg/L. Only one value for the ^{226}Ra content is available—33 pg/L. SO_4-free brines of a pre-Tortonian hot climate recharge are also characterized by high mineralization, variable Ba and Sr content, and ^{226}Ra contents of up to 3100 pg/L. The oldest paleoinfiltration brines, assumed to be of Permian age and it could have a salinity of up to 230 g/L. They do not contain U and $SO_4{}^{2-}$, but they are extremely rich in Ba^{2+} (up to 1800 mg/L), Sr^{2+} (up to 450 mg/L), and ^{226}Ra (up to 6000 pg/L). Finally, mixed waters are waters affected by the mixing of any other types, mainly due to coal mining activities [49].

3. Materials and Methods

The piece of old water pipe in question came from the 10th floor of the Doubrava Shaft. It was used for pumping waste water to the main pumping station in the by-pass of the 10th floor. The investigated material forms a beige precipitate crust (“scale”) that is several centimetres thick. It is porous and shows indications of a botryoidal surface (Figure 2).

X-ray powder diffraction measurements were conducted while using a Bruker-AXS D8 Advance instrument (Institute of Geological Engineering, VŠB-Technical University of Ostrava, operator D. Matýsek) with 2θ/θ geometry and measured using a LynxEye position sensitive detector under the following conditions: radiation: CoKα/Fe filter, voltage: 40 kV, current: 40 mA, step-by-step mode of 0.014° 2θ with an interval of 0.25 s per step, and the summation of at least five successive measurements based on the complexity of the recording. The samples were prepared by pulverisation in an agate mortar and transfer onto a low-background silicon holder. The data were digitally processed while using Bruker Diffrac Suite software (Bruker Corporation, Billerica, MA, USA). The Rietveld method in Bruker Topas version 4.2 was used to verify the accuracy of the qualitative evaluation of the measurements.

Wavelength-dispersive X-ray spectroscopic analyses (WDS) were performed at the Laboratory of Electron Microscopy and Microanalysis at the Faculty of Science at Masaryk University in Brno on an electron microprobe (model CAMECA SX100 and analyst R. Čopjaková). The standards used were leucite (Rb Lα), $SrSO_4$ (Sr Kα, S Kα), $MgAl_2O_4$ (Mg Kα), fluorapatite (P Kα), wollastonite (Ca Kα), orthoclase (K Kα), almandine (Fe Kα), baryte (Ba Lα), vanadinite (Cl Kα), titanite (Si Kα), and andalusite (Al Kα). 15 kV and 10 nA were the measuring conditions, with a spot 10 µm in size and a graphite coating.

Figure 2. Example of beige incrustation from a drainage pipe with Ra-rich baryte. Size 6 × 5 cm^2.

Two samples of the Ra-rich baryte powder were prepared and then analysed for their ^{226}Ra content. The first sample, containing m = 4.47(2) g of the Ra-rich baryte powder, was mixed with 1.90(1) mL of ^{226}Ra water solution of known activity, A_0 = 2712(24) Bq, provided by Eurostandard, Czech Republic. The second sample, which contained the same amount (4.47 g) of the Ba powder, was mixed with 1.90(1) mL of distilled water. Both of the samples were sealed in 5 mL polyethylene containers while using a special wax to prevent ^{222}Rn leakage and left for 28 days to establish secular equilibrium between ^{226}Ra and its decay products ^{222}Rn, ^{214}Pb, and ^{214}Bi. The gamma spectra of the samples were then measured using a 30% HPGe spectrometer (GC3018, Canberra) equipped with 10 cm lead + 1 mm cadmium + 1 mm copper shielding to reduce the background. The spectra were analysed while using Genie2000 software (Mirion Technologies, Canberra, Australia).

The two-sample method enables the determination of ^{226}Ra activity without the need to calibrate the gamma spectrometer. There is also no need to make corrections for gamma self-absorption in the samples. We only assume that the ^{226}Ra activities of both samples, A_1 and A_2, are homogeneously distributed. For the five most intensive gamma lines from the ^{226}Ra decay chain (295.22 keV: ^{214}Pb decay, 351.93 keV: ^{214}Pb decay, 609.31 keV: ^{214}Bi decay, 1120.29 keV: ^{214}Bi decay, and 1764.49 keV: ^{214}Bi decay; the gamma line from the ^{226}Ra decay at 186.21 keV cannot be used, because it is contaminated by a close-lying line at 185.72 keV from ^{235}U decay [50], we can write:

$$R_1 - R_B = \epsilon\,(A + A_0) \qquad \text{and} \qquad R_2 - R_B = \epsilon\,A, \tag{1}$$

where R_1 and R_2 are the detected gamma rates for the first and the second samples, respectively, R_B is the background gamma rate, and ϵ is the detection efficiency. The unknown ^{226}Ra activity can then be calculated from:

$$A = A_0(R_2 - R_B)/(R_1 - R_2) \tag{2}$$

The specific activity A_m is then obtained from $A_m = A/m$. The standard uncertainties of the measured quantities are shown in parentheses, and the standard uncertainties of the calculated quantities are obtained from the Gaussian law of uncertainty propagation.

The analyses of water were performed in the accredited labs of Labtech Company. The acid-base reaction was measured with an Orion pH meter (Model 710A), and the total mineralization of the individual samples of water was determined by the gravimetric method. The contents of major anions (Cl^- and SO_4^{2-}) were established by ion chromatography while using an IC 90 chromatograph that was manufactured by Dionex Co (Sunnyvale, CA, USA). Iodides and bromides were determined by redox titration, and the concentrations of cations and heavy metals (Ca, Mg, Na, K, Li, Al, Fe, Ba, and Sr) were determined by the ICP-OES method while using an Jobin Activa spectrometer. The contents of the CO_2 fixation forms were calculated from their neutralizing capacities while using an acid-base titration method.

4. Results

Powder X-ray diffraction revealed that baryte is the prevailing constituent of the precipitate (scale). The precipitate also contains traces of kaolinite and quartz and also possibly an amorphous phase containing iron. The cell parameters calculated using the Rietveld method correspond with data given in the literature for substituted baryte (Table 1). The difference in the "a" axis can be ascribed to the substitution of Sr into the Ba positions of the crystal lattice of baryte, which causes the shrinking of the "a" distance of the unit cell [51], and possibly also to substitution of Ca into the same position [52].

Table 1. Comparison of the cell parameters of the investigated baryte with previously published data.

Source	a (Å)	b (Å)	c (Å)
this study	8.8089(2)	5.4457(1)	7.1231(1)
[53]	8.884(2) [1]	5.457(3) [1]	7.157(2) [1]
[54]	8.88101(3) [1]	5.45447(1) [1]	7.15505(1) [1]

[1] Axis labelled differently in the cited works.

Table 2 gives the chemical composition of studied precipitate, since the pure baryte spots could not be measured to their thickness (Figure 3) and porosity of the aggregate. This factor also affected the totals of the measurement. We ascribed content of K, Fe, P, Si, Al, and Cl to detected minor amounts of kaolinite, quartz, and amorphous Fe-bearing phase. Empirical formula $(Ba_{0.934}Sr_{0.058}Ca_{0.051}Mg_{0.003})_{\Sigma 1.046}S_{0.985}O_{4.000}$ given as the mean of seven determinations (Table 2) correspond well with the ideal baryte. The major isomorphic admixtures are Sr and Ca (both up to 0.06 *apfu*), and there is also minor content of Mg (up to 0.01 *apfu*).

Table 2. Chemical composition of studied precipitate and empirical formula of baryte based on 4 oxygens per formula unit.

Constituent	Mean	1	2	3	4	5	6	7
BaO	57.06	55.73	57.19	58.85	58.30	56.44	57.30	55.60
SrO	2.37	2.37	2.63	2.15	2.35	2.23	2.56	2.32
RbO	0.02	b.d.l.[1]	b.d.l.[1]	b.d.l.[1]	b.d.l.[1]	b.d.l.[1]	0.11	b.d.l.[1]
MgO	0.05	0.02	0.07	0.04	0.03	0.03	0.04	0.08
CaO	1.14	1.07	1.06	1.11	1.25	1.26	1.08	1.15
K_2O	0.19	0.27	0.20	0.14	0.16	0.22	0.13	0.18
Al_2O_3	1.01	1.53	1.17	0.71	0.71	1.00	0.90	1.07
Fe_2O_3	2.72	3.39	2.25	1.43	1.61	2.86	2.70	4.81
SiO_2	1.23	1.65	1.37	0.73	0.74	1.24	1.40	1.47
SO_3	31.41	30.27	30.69	32.43	32.71	31.37	32.15	30.25
Cl	0.15	0.17	0.11	0.16	0.10	0.20	0.05	0.25

Table 2. *Cont.*

Constituent	Mean	1	2	3	4	5	6	7
Σ	97.35	96.47	96.76	97.79	97.97	96.85	98.43	97.20
Ba^{2+}	0.934	0.944	0.951	0.936	0.921	0.927	0.921	0.941
Sr^{2+}	0.058	0.059	0.065	0.051	0.055	0.054	0.061	0.058
Rb^{2+}	0.000	0.000	0.000	0.000	0.000	0.000	0.003	0.000
Mg^{2+}	0.003	0.001	0.004	0.002	0.002	0.002	0.002	0.005
Ca^{2+}	0.051	0.050	0.048	0.048	0.054	0.056	0.048	0.053
S^{6+}	0.985	0.982	0.977	0.988	0.989	0.987	0.989	0.981

[1] b.d.l.—below detection limit.

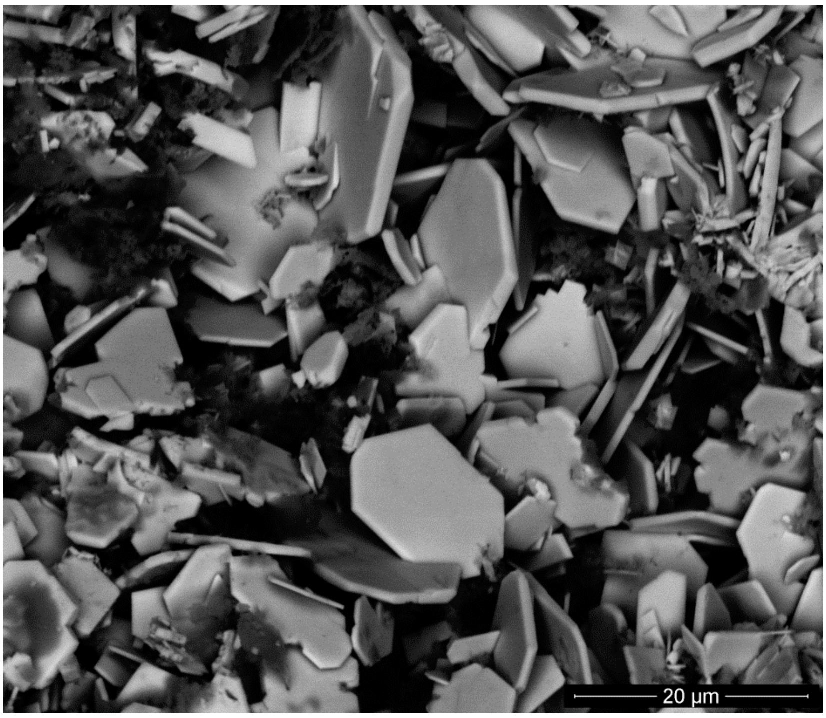

Figure 3. Backscattered electron (BSE) image of the baryte aggregate.

The two-sample method described in Section 3 enabled us to determine the ^{226}Ra activity and specific activity for the five most intensive gamma lines from the ^{226}Ra decay chain (Table 3). The weighted arithmetic mean of the specific activity of ^{226}Ra calculated from all five detected gamma lines equals 39.62(22) Bq/g (Table 3). If we consider an older non-SI unit of radioactivity, the curie (Ci), which corresponds to 3.7×10^{10} decays per second of 1 g ^{226}Ra [55], then the content of radium ^{226}Ra in the baryte is 1.071 ng/g.

Table 3. Detected gamma rates R_1, R_2, and R_B (first and second sample and background, respectively) for the five most intensive gamma lines and the calculated ^{226}Ra activities A and specific activities A_m. Combined standard uncertainties are shown in parentheses.

Nuclide	Energy	R_1	R_2	R_B	A	A_m
	(keV)	s^{-1}	s^{-1}	s^{-1}	Bq	Bq/g
^{214}Pb	295.22	20.372(62)	1.2509(51)	not detected	177.4(19)	39.69(48)
^{214}Pb	351.93	34.229(69)	2.1115(64)	0.00192(62)	178.1(18)	39.84(43)
^{214}Bi	609.31	23.502(71)	1.4378(58)	0.00154(55)	176.5(20)	39.49(47)
^{214}Bi	1120.29	4.663(33)	0.2883(32)	not detected	178.7(29)	39.98(67)
^{214}Bi	1764.49	3.780(23)	0.2295(21)	0.00159(26)	174.1(27)	38.95(61)

The known activity of ^{226}Ra in the two samples was used for the efficiency calibration of the HPGe spectrometer that enabled us to determine the activity of the other two radium isotopes from the ^{232}Th series that were identified in the samples, namely ^{228}Ra and ^{224}Ra (Table 4). The weighted arithmetic means of the specific activity of ^{228}Ra calculated from the two detected gamma lines (from the ^{228}Ac decay) equals 23.39(26) Bq/g. For ^{224}Ra (from ^{212}Pb and ^{212}Bi decays), we get 11.03(25) Bq/g. The ratios of the specific activities of ^{226}Ra and ^{228}Ra, and ^{224}Ra and ^{228}Ra then equal 1.694(21) and 0.472(12), respectively. It should be noted that the latter ratio is identical to the ratio of specific activities of ^{228}Th and ^{228}Ra.

Table 4. Background corrected ^{228}Ra (from ^{228}Ac) and ^{224}Ra (from ^{212}Pb and ^{212}Bi) activities A_1, A_2 and specific activities A_{1m}, A_{2m} (first and second sample, respectively). Combined standard uncertainties are shown in parentheses.

Nuclide	**Energy**	$\mathbf{A_1}$	$\mathbf{A_2}$	$\mathbf{A_{1m}}$	$\mathbf{A_{2m}}$
	(keV)	Bq	Bq	Bq/g	Bq/g
^{212}Pb	238.63	48.6(20)	49.6(15)	10.87(46)	11.10(34)
^{212}Pb	300.09	not detected	49.1(25)	-	10.98(57)
^{228}Ac	911.20	110.8(67)	105.4(14)	24.8(15)	23.56(33)
^{228}Ac	968.97	101.3(81)	103.0(18)	22.7(19)	23.04(42)
^{212}Bi	1620.74	not detected	53.9(76)	-	12.1(18)

The analysed mine water samples (P2307 and P41 in Table 5) indicate Miocene brines. Typically, the SO_4^{2-} concentrations are below the detection limit. However, Br/I is much higher than the range that was published by [49], so they may, in fact, belong to the group of SO_4-free brines of a pre-Tortonian hot climate recharge. Samples P2111, P1804, and P4505 in Table 4 represent mixed brines from mine works with sulfate efflorescences. An increased SO_4^{2-} content is typical for them. Depletion in Ba and Sr is an effect of the precipitation of baryte.

Table 5. Geochemical composition of the selected mine waters from the ČSA Mine, Doubrava Shaft.

Sample No.	**Unit**	**P2307**	**P41**	**P2111**	**P1804**	**P4505**
pH		7.1	6.0	6.4	7.4	7.3
mineralization	mg/L	112,000	127,000	39,100	281,000	35,900
anions						
Cl^-	mg/L	68,900	79,900	23,900	134,000	21,200
Br^-	mg/L	369	391	111	217	100
I^-	mg/L	10.1	8.9	11.3	14.1	7.9
SO_4^{2-}	mg/L	<10	<10	113	222	677
HCO_3^-	mg/L	62.2	<24	293	48.2	162
CO_3^{2-}	mg/L	<24	<24	<24	<24	<24
cations						
Na^+	mg/L	32,400	34,900	12,400	142,000	12,000
K^+	mg/L	554	515	214	438	284
Ca^{2+}	mg/L	7340	8690	1370	3000	1250
Mg^{2+}	mg/L	1810	2100	604	642	249
Fe_{tot}	mg/L	<0.05	4.62	41.20	<0.05	0.075
Mn^{2+}	mg/L	2.69	7.20	2.18	4.45	0.67
Sr^{2+}	mg/L	286	286	47	84	32
Ba^{2+}	mg/L	521	323	2	5	0.7
Li^+	mg/L	11.2	9.1	3.5	9.6	3.0
Al^{3+}	mg/L	<0.03	<0.15	<0.03	<0.03	<0.03
NH^{4+}	mg/L	18.59	33.93	13.48	22.45	15.45

5. Discussion

The examples of the mine water chemical composition (Table 5) reveal the story behind the radium-rich baryte. Original Miocene brines are rich in Ba, Sr, and Ra, but are virtually SO_4 free.

Radium, especially ^{226}Ra and ^{228}Ra, is generated by the alpha decay of ^{238}U, respectively ^{232}Th from accessory minerals (zircon, monazite, and apatite). Alpha recoil is the process that concentrates ^{226}Ra and ^{228}Ra in the brines [56]. Rock massif is oxygen deficient, and water can also contain free CH_4 from natural coal degassing, so it does not cause sulfide decomposition. Once the water reaches the mine works, which have different geochemical conditions, it combines with bacterial activity to participate in sulfide decomposition in both the coal and surrounding rocks [57]. Typically, the $SO_4{}^{2-}$ content is increased. Ba reacts with sulfate anions and precipitates as baryte once such waters of divergent composition are mixed. Strontium and radium are hence incorporated into its crystal lattice as isomorphic admixtures due to their similar ionic radius and coordination number.

Similar findings have also been reported from the Polish part of the Upper Silesian Basin. Radium-rich mine waters are present, according to [49], and they pose a possible hazard to the environment, since ca. one-half of the radioactive nuclides (mostly radium) flowing into the mines are discharged to surface waters [58]. There, the radioactive nuclides become part of the sediment, fixed in baryte, witherite ($BaCO_3$), or metal oxyhydroxides [59]. However, we were able to document and describe what happens to radionuclides that do not leave the underground mines. Radium is at least partly fixed in baryte, and, with some exceptions, such as the possible recycling of the steel parts of water drainage and pumping systems, the baryte does not enter surface ecosystems, due to spontaneous water mixing. Baryte is considered a relatively stable mineral [60,61] and it should not release radium after the closure of mines and their flooding. Therefore, the spontaneous precipitation of Ra-rich baryte is the natural analogue of the treatment method tested by [62] for radium removal from mine waters. However, radium that is fixed in baryte could be released by activities of sulfate-reducing bacteria [63], reported from both laboratory [64–66] and field [66] environments.

6. Conclusions

Radium is a significant environmental pollutant. The isotope ^{226}Ra is the most significant, while considering its long half-life (1600 years), radioactivity, toxicity, and ability to be incorporated into animal and human bones due to its geochemical similarity with calcium [67]. Bituminous coal mining in the Upper Silesian Basin presents a substantial source of Ra. This element could enter terrestrial aquatic and atmospheric environments due to the pumping of radium-rich brines. The spontaneous fixation of ^{226}Ra in Ra-rich baryte due to the mixing of waters of different chemical nature is beneficial if it occurs underground, because the radium is fixed far from possible entry points to biogenic cycles or contact with living organisms. Experiments have shown that similar processes, i.e., blending Ra-bearing fluids with acid mine drainage (AMD) waters, could be used to remove radium and barium from hydraulic fracturing fluids [68] or mine waters [62]. However, the evaluation of radiation hazards for miners would require a separate study, since there are many factors that affect the precise place of baryte precipitation, presence of miners at those locations, and handling with the material containing precipitate.

Author Contributions: Conceptualization, J.J. and D.M.; methodology, J.J., D.M., and P.A.; formal analysis, J.J.; investigation, J.J., D.M., P.A., R.U.; resources, M.O. and J.J.; writing—original draft preparation, J.J., P.A., and M.O.; writing—review and editing, J.J. and M.S.; supervision, J.J.; funding acquisition, J.J. and P.A. All authors have read and agreed to the published version of the manuscript.

Funding: This research was supported by "Ministry of Education, Youth, and Sports of the Czech Republic, grant numbers SP2019/26, SP2019/77, and MSMT-15304/2017-1, INTER-EXCELLENCE LTC17051 European Anthroposhere as a Source of Mineral Raw Materials".

Acknowledgments: The authors are grateful to P. Količová for preparing the samples for the radium analysis and to the three anonymous reviewers, whose comments and suggestions helped to improve the scientific content of the paper.

Conflicts of Interest: The authors declare no conflict of interest.

References

1. Rutherford, E.V. Bakerian lecture: The succession of changes in radioactive bodies. *Phil. Trans. A* **1904**, *204*, 169–219.
2. Calabrese, E.J. Excessive barium and radium-226 in Illinois drinking water. *J. Environ. Health.* **1977**, *39*, 366–369. [PubMed]
3. Mokrik, R.; Karro, E.; Savitskaja, L.; Drevaliene, G. The origin of barium in the Cambrian-Vendian aquifer system, North Estonia. *Est. J. Earth Sci.* **2009**, *58*, 193–208. [CrossRef]
4. Fry, L.M. Radium and fission products radioactivity in thermal waters. *Nature* **1962**, *195*, 375–376. [CrossRef]
5. Laboutka, M.; Vylita, B. Mineral and thermal waters of Western Bohemia. *GeoJournal* **1983**, *7*, 403–411. [CrossRef]
6. Sturchio, N.C.; Bohlke, J.K.; Markun, F.J. Radium isotope geochemistry of thermal waters, Yellowstone National Park, Wyoming, USA. *Geochim. Cosmochim. Acta* **1993**, *57*, 1203–1214. [CrossRef]
7. Bayés, J.C.; Gómez, E.; Garcias, F.; Casas, M.; Cerdá, V. Radium determination in mineral waters. *Appl. Radiat. Isot.* **1996**, *47*, 849–853. [CrossRef]
8. Bituh, T.; Marovic, G.; Petrinec, B.; Sencar, J.; Franulovic, I. Natural radioactivity of ^{226}Ra and ^{228}Ra thermal and mineral waters in Croatia. *Radiat. Prot. Dosim.* **2009**, *133*, 119–123. [CrossRef]
9. Condomines, M.; Gourdin, E.; Gataniou, D.; Seidel, J.-L. Geochemical behavior of radium isotopes and radon in a coastal thermal system (Balaruc-les-Bains, South of France). *Geochim. Cosmochim. Acta* **2012**, *98*, 160–176. [CrossRef]
10. Kamenova-Totzeva, R.; Totzev, A.; Kotova, R. Radium content in Bulgarian mineral waters. *Nucl. Technol. Radiat.* **2018**, *33*, 133–138. [CrossRef]
11. Herczog, A.L.; Simpson, H.J.; Anderson, R.F.; Trier, R.M.; Mathieu, G.G.; Deck, B.L. Uranium and radium mobility in groundwaters and brines within the Delaware Basin, Southeastern New Mexico, U.S.A. *Chem. Geol.* **1988**, *72*, 181–196.
12. Dickson, B.L. Radium in groundwater. In *The Environmental Behavior of Radium*; International Atomic Energy Agency: Vienna, Austria, 1990; Volume 1, pp. 335–372.
13. Kozłowska, B.; Walencik, A.; Przylibski, T.A.; Dorda, J.; Zipper, W. Uranium, radium and radon isotopes in selected brines of Poland. *Nukleonika* **2010**, *55*, 519–522.
14. Kraemer, T.F.; Wood, W.W.; Sanford, W.E. Distinguishing seawater from geologic brine in saline coastal groundwater using radium-226; an example from the Sabkha of the UAE. *Chem. Geol.* **2014**, *371*, 1–8. [CrossRef]
15. Řanda, Z.; Ulrych, J.; Turek, K.; Mihaljevič, M.; Adamovič, J.; Mizera, J. Radiobarites from the Cenozoic volcanic region of the Bohemian Massif: Radiochemical study, history, and leas isotopic composition. *J. Radioanal. Nucl. Chem.* **2010**, *283*, 89–94. [CrossRef]
16. Ulrych, J.; Adamovič, J.; Žák, K.; Frána, J.; Řanda, Z.; Langrová, A.; Skála, R.; Chvátal, M. Cenozoic "radiobarite" occurrences in the Ohře (Eger) Rift, Bohemian Massif: Mineralogical and geochemical revision. *Chem. der Erde-Geochem.* **2007**, *67*, 301–312. [CrossRef]
17. Grandia, F.; Merino, J.; Amphos, J.B. *Assessment of the Radium-Barium Co-Precipitation and its Potential Influence on the Solubility of Ra in the Near-Field*; Svensk Kärnbränslehantering AB: Stockholm, Sweden, 2008.
18. Zielinski, R.A.; Otton, J.K. *Naturally Occurring Radioactive Material (NORM) in Produced Water and Oil-Field Equipment—An Issue for the Energy Industry*; U.S. Geological Survey: Reston, VA, USA, 1999.
19. Zielinski, R.A.; Otton, J.K.; Budahn, J.R. Use of radium isotopes to determine the age and origin of radioactive barite at oil-field production sites. *Environ. Pollut.* **2001**, *113*, 299–309. [CrossRef]
20. Matta, L.E.; Godoy, J.M.; Reis, M.C. ^{226}Ra, ^{228}Ra and ^{228}Th in scale and sludge samples from the Campos Basin oilfield E&P activities. *Radiat. Prot. Dosim.* **2002**, *102*, 175–178.
21. Omar, M.; Ali, H.M.; Abu, M.P.; Kontol, K.M.; Ahmad, Z.; Ahmad, S.H.S.S.; Sulaiman, I.; Hamzah, R. Distribution of radium in oil and gas industry wastes from Malaysia. *Appl. Radioact. Isotopes* **2004**, *60*, 779–782. [CrossRef]
22. Parmaksiz, A.; Ağuş, Y.; Bulgurlu, F.; Bulur, T.; Öncü, T.; Özkök, Y.Ö. Measurement of enhanced radium isotopes in oil production wastes in Turkey. *J. Environ. Radioactiv.* **2015**, *141*, 82–89. [CrossRef]
23. Seeley, F.G. Problems in the separation of radium from uranium ore tailings. *Hydrometallurgy* **1977**, *2*, 249–263. [CrossRef]

24. Nirdosh, I.; Muthuswami, S.V.; Baird, M.H.I. Radium in uranium mill tailings—Some observations on retention and removal. *Hydrometallurgy* **1984**, *12*, 151–176. [CrossRef]
25. de Jesus, A.S.M. Technological enhancement. In *The Behavior of Radium in Waterways and Aquifers*; International Atomic Energy Agency: Vienna, Austria, 1984; pp. 87–115.
26. Martin, A.; Crusius, J.; McNee, J.J.; Yanful, E. The mobility of radium-226 and trace metals in pre-oxidized subaqueous uranium mill tailings. *Appl. Geochem.* **2003**, *18*, 1095–1110. [CrossRef]
27. Lardinoye, M.H.; Weterings, K.; van de Berg, W.B. Unexpected ^{226}Ra build-up in wet-process phosphoric-acid plants. *Health Phys.* **1982**, *42*, 503–514. [CrossRef] [PubMed]
28. Rutherford, P.M.; Dudas, M.J.; Arocena, J.M. Heterogenous distribution of radionuclides, barium and strontium in phosphogypsum by-product. *Sci. Total Environ.* **1996**, *180*, 201–209. [CrossRef]
29. Burnett, W.C.; Elzerman, A.W. Nuclide migration and the environmental radiochemistry of Florida phosphogypsum. *J. Environ. Radioactiv.* **2001**, *54*, 27–51. [CrossRef]
30. Sahu, S.K.; Ajmal, P.Y.; Bhangare, R.C.; Tiwari, M.; Pandit, G.G. Natural radioactivity assessment of a phosphate fertilizer plant area. *J. Radiat. Res. Appl. Sci.* **2014**, *7*, 123–128. [CrossRef]
31. Martin, P.; Akber, R.A. Radium isotopes as indicators of adsorption-desorption interactions and barite formation in groundwater. *J. Environ. Radioactiv.* **1999**, *46*, 271–286. [CrossRef]
32. Zhu, C. Coprecipitation in the barite isostructural family: 1. Binary mixing properties. *Geochim. Cosmochim. Acta* **2004**, *68*, 3327–3337. [CrossRef]
33. Curti, E.; Fujiwara, K.; Iijima, K.; Tits, J.; Cuesta, C.; Kitamura, A.; Glaus, M.A.; Müller, W. Radium uptake during barite recrystallization at 23 ± 2 °C as a function of solution composition: An experimental ^{133}Ba and ^{226}Ra tracer study. *Geochim. Cosmochim. Acta* **2010**, *74*, 3553–3570. [CrossRef]
34. Rosenberg, Y.O.; Metz, V.; Oren, Y.; Volkman, Y.; Ganor, J. Co-precipitation of radium in high ionic strength systems: 2. Kinetic and ionic strength effect. *Geochim. Cosmochim. Acta* **2011**, *75*, 5403–5422. [CrossRef]
35. Kumpera, O.; Martinec, P. The development of the Carboniferous accretionary wedge in the Moravian-Silesian Paleozoic Basin. *J. Czech Geol. Soc.* **1995**, *40*, 47–64.
36. Dopita, M.; Kumpera, O. Geology of the Ostrava-Karviná coalfield, Upper Silesian Basin, Czech Republic, and its influence on mining. *Int. J. Coal Geol.* **1993**, *23*, 291–321. [CrossRef]
37. Dopita, M. (Ed.) *Geology of the Czech part of the Upper Silesian Basin*; Ministerstvo životního prostředí ČR: Praha, Czech Republic, 1997. (In Czech with English summary)
38. Pešek, J.; Sivek, M. *Coal-Bearing Basins and Coal Deposits of the Czech Republic*; Czech Geological Survey: Prague, Czech Republic, 2016.
39. Jirásek, J.; Opluštil, S.; Sivek, M.; Schmitz, M.D.; Abels, H.A. Astronomical forcing of Carboniferous paralic sedimentary cycles in the Upper Silesian Basin, Czech Republic (Serpukhovian, latest Mississippian): New radiometric ages afford an astronomical age model for European biozonations and substages. *Earth-Sci. Rev.* **2018**, *177*, 715–741. [CrossRef]
40. Jirásek, J.; Hýlová, L.; Sivek, M.; Jureczka, J.; Martínek, K.; Sýkorová, I.; Schmitz, M. The Main Ostrava Whetstone: Composition, sedimentary processes, palaeogeography and geochronology of a major Mississippian volcaniclastic unit of the Upper Silesin Basin (Poland and Czech Republic). *Int. J. Earth Sci.* **2013**, *102*, 989–1006. [CrossRef]
41. Opluštil, S.; Lojka, R.; Rosenau, N.; Strnad, L.; Kędzior, A. Climatically-driven cyclicity and peat formation in fluvial setting of the Moscovian—Early Kasimovian Cracow Sandstone Series, Upper Silesia (Poland). *Int. J. Coal Geol.* **2019**, *212*, 103234. [CrossRef]
42. Kalvoda, J.; Babek, O.; Fatka, O.; Leichmann, J.; Melichar, R.; Nehyba, S.; Spacek, P. Brunovistulian terrane (Bohemian Massif, Central Europe) from late Proterozoic to late Paleozoic: A review. *Int. J. Earth Sci.* **2008**, *97*, 497–518. [CrossRef]
43. Buła, Z.; Habryn, R.; Jachowict-Zdanowska, M.; Żaba, J. Precambrian and Lower Paleozoic of the Brunovistulicum (eastern part of the Upper Silesian Block, southern Poland)—The state of the art. *Geol. Q.* **2015**, *59*, 123–134. [CrossRef]
44. Pešek, J.; Sýkorová, I.; Jelínek, J.; Michna, O.; Forstová, J.; Martínek, K.; Vašíček, M.; Havelcová, M. Major and minor elements in the hard coal from the Czech Upper Paleozoic basins. *Czech Geol. Surv. Spec. Pap.* **2010**, *20*, 1–40.
45. Ketris, M.P.; Yudovich, Y.E. Estimations of Clarkes for carbonaceous biolithes: World averages for trace element contents in black shales and coals. *Int. J. Coal Geol.* **2009**, *78*, 135–148. [CrossRef]

46. René, M. Distribution of uranium, thorium and gold in Carboniferous sediments in the NE part of the Bohemian Massif. *Čas. Slez. Muz. Ser. A* **1992**, *41*, 151–157. (In Czech with English abstract)
47. Dopita, M.; Králík, J. *Coal tonsteins of Ostrava-Karviná Coal Basin*; OKD: Ostrava, Czechoslovakia, 1977. (In Czech with English and Russian summary)
48. Grmela, A. Hydrogeological conditions. In *Geologie České Části Hornoslezské Pánve*; Dopita, M., Ed.; Ministerstvo životního prostředí České republiky: Praha, Czech Republic, 1997; pp. 198–204. (In Czech with English summary).
49. Pluta, I.; Zuber, A. Origin of brines in the Upper Silesian Coal Basin (Poland) inferred from stable isotope and chemical data. *Appl. Geochem.* **1995**, *10*, 447–460. [CrossRef]
50. Gilmore, G. *Practical Gamma-Ray Spectrometry*, 2nd ed.; John Willey & Sons Ltd.: Chichester, England, 2007.
51. Goldish, E. X-ray diffraction analysis of barium-strontium sulfate (barite-celestite) solid solutions. *Powder Diffr.* **1989**, *4*, 214–216. [CrossRef]
52. Hennessy, A.J.B.; Graham, G.M. The effect of additives on the co-crystalisation of calcium with barium sulphate. *J. Cryst. Growth* **2002**, *237–239*, 2153–2159. [CrossRef]
53. Miyake, M.; Minato, I.; Morikawa, H.; Iwai, S. Crystal structures and sulphate force constants of barite, celestite, and anglesite. *Am. Mineral.* **1978**, *63*, 506–510.
54. Antao, S.M. Structural trends for celestite ($SrSO_4$), anglesite ($PbSO_4$), and barite ($BaSO_4$): Confirmation of expected variations within the SO_4 groups. *Am. Mineral.* **2012**, *97*, 661–665. [CrossRef]
55. Knoll, G.F. *Radiation Detection and Measurement*, 3rd ed.; John Willey & Sons Inc.: New York, NY, USA, 2000.
56. Eggeling, L.; Genter, A.; Kölbel, T.; Münch, W. Impact of natural radionuclides on geothermal exploitation in the Upper Rhine Graben. *Geothermics* **2013**, *47*, 80–88. [CrossRef]
57. Matýsek, D.; Jirásek, J.; Osovský, M.; Skupien, P. Minerals formed by the weathering of sulfides in miners of the Czech part of the Upper Silesian Basin. *Mineral. Mag.* **2014**, *78*, 1265–1286. [CrossRef]
58. Wysocka, M.; Chalupnik, S.; Chmiellewska, I.; Janson, E.; Radziejowski, W.; Samolej, K. Natural radioactivity in Polish coal mines: An attempt to assess the trend of radium release into the environment. *Mine Water Environ.* **2019**, *38*, 581–589. [CrossRef]
59. Courbet, C.; Wysocka, M.; Martin, L.; Chmielewska, I.; Bonczyk, M.; Michalik, B.; Barker, E.; Zebracki, M.; Mangeret, A. Fate of radium in river and lake sediments impacted by coal mining sites in Silesia (Poland). In *Proceedings IMWA 2016—Mining Meets Water—Conflicts and Solutions*; Drebenstedt, C., Paul, M., Eds.; TU Bergakademie Freiberg: Freiberg, Germany, 2016; pp. 1249–1253.
60. Hanor, J.S. Barite–celestine geochemistry and environments of formation. *Rev. Mineral. Geochem.* **2000**, *40*, 193–275. [CrossRef]
61. Ptacek, C.; Blowees, D. Predicting sulfate-mineral solubility in concentrated waters. *Rev. Mineral. Geochem.* **2000**, *40*, 513–540. [CrossRef]
62. Chałupnik, S.; Wysocka, M. Radium removal from mine waters in underground treatment installations. *J. Environ. Radioactiv.* **2008**, *99*, 1548–1552. [CrossRef] [PubMed]
63. Singleton, R. The sulfate-reducing bacteria: An overview. In *The Sulfate-Reducing Bacteria: Contemporary Perspectives*; Odom, J.M., Singleton, R., Eds.; Brock/Springer Series in Contemporary Bioscience; Springer: New York, NY, USA, 1993; pp. 1–20.
64. Landa, E.R. Mobilization of radionuclides from uranium mill tailings and related waste materials in anaerobic environmens. *J. Radioanal. Nucl. Chem.* **2003**, *255*, 559–563. [CrossRef]
65. Larock, P.; Hyun, J.-H.; Boutelle, S.; Burnett, W.C.; Hull, C.D. Bacterial mobilization of polonium. *Geochim. Cosmochim. Acta* **1996**, *60*, 4321–4328. [CrossRef]
66. Phillips, E.J.P.; Landa, E.R.; Kraemer, T.F.; Zielinski, R.A. Sulfate-reducing bacteria release barium and radium from naturally occurring radioactive material in oil-field barite. *Geomicrobiol. J.* **2001**, *18*, 167–182. [CrossRef]
67. Iyengar, M.A.R. The natural distribution of radium. In *The Environmental Behavior of Radium*; International Atomic Energy Agency: Vienna, Austria, 1990; Volume 1, pp. 59–128.
68. Kondash, A.J.; Warner, N.R.; Lahav, O.; Vengosh, A. Radium and barium removal through blending hydraulic fracturing fluids with acid mine drainage. *Environ. Sci. Technol.* **2014**, *48*, 1334–1342. [CrossRef] [PubMed]